ADVANCED FUNCTIONAL MATERIALS
www.afm-journal.de

The Role of Chlorine in the Formation Process of "$CH_3NH_3PbI_{3-x}Cl_x$" Perovskite

*Hui Yu, Feng Wang, Fangyan Xie, Wenwu Li, Jian Chen, and Ni Zhao**

$CH_3NH_3PbI_{3-x}Cl_x$ is a commonly used chemical formula to represent the methylammonium lead halide perovskite fabricated from mixed chlorine- and iodine-containing salt precursors. Despite the rapid progress in improving its photovoltaic efficiency, fundamental questions remain regarding the atomic ratio of Cl in the perovskite as well as the reaction mechanism that leads to its formation and crystallization. In this work we investigated these questions through a combination of chemical, morphological, structural and thermal characterizations. The elemental analyses reveal unambiguously the negligible amount of Cl atoms in the $CH_3NH_3PbI_{3-x}Cl_x$ perovskite. By studying the thermal characteristics of methylammonium halides as well as the annealing process in a polymer/perovskite/FTO glass structure, we show that the formation of the $CH_3NH_3PbI_{3-x}Cl_x$ perovskite is likely driven by release of gaseous CH_3NH_3Cl (or other organic chlorides) through an intermediate organometal mixed halide phase. Furthermore, the comparative study on $CH_3NH_3I/PbCl_2$ and CH_3NH_3I/PbI_2 precursor combinations with different molar ratios suggest that the initial introduction of a $CH_3NH_3^+$ rich environment is critical to slow down the perovskite formation process and thus improve the growth of the crystal domains during annealing; accordingly, the function of Cl^- is to facilitate the release of excess $CH_3NH_3^+$ at a relatively low annealing temperatures.

1. Introduction

Recently organometal halide perovskites have emerged as a promising photovoltaic (PV) material that exhibits high power conversion efficiency (PCE) as well as low-temperature processibility.[1–4] Among various perovskites, the methylammonium lead halide perovskites ($MAPbX_3$), such as, $CH_3NH_3PbI_3$,[5,6] $CH_3NH_3PbI_{3-x}Cl_x$,[7,8] and $CH_3NH_3PbBr_3$,[9,10] have been studied most extensively due to their wide absorption range (visible-to-near infrared) and excellent electronic properties. When used for PV applications, $CH_3NH_3PbI_3$ is often combined with mesostructured cells to achieve good device performance, whereas $CH_3NH_3PbI_{3-x}Cl_x$ can yield high PCEs in a planar device structure and through a simple spin-coating or co-evaporation film deposition process.[11–17] Very recently there have been studies showing high-performance planar $CH_3NH_3PbI_3$ solar cells, however, the device fabrication requires more complicated solution processes.[18,19] It has been broadly observed that the PCE of perovskite solar cells is closely related to the morphology and crystal structure of the perovskite absorbers.[20–23] Accordingly, the film growth parameters, such as the molar ratio and concentration of the precursor solutions as well as the annealing temperature and duration, have to be carefully designed.

In this work we focus on the growth process of the $MAPbX_3$ perovskite absorber prepared from mixed chlorine- and iodine-containing precursors, which is therefore often referred as $CH_3NH_3PbI_{3-x}Cl_x$. Commonly, the $CH_3NH_3PbI_{3-x}Cl_x$ films are prepared by spin-coating a precursor solution of CH_3NH_3I and $PbCl_2$ in dimethylformamide (DMF) at a 3:1 molar ratio, followed by thermal annealing at around 100 °C.[16] The PCEs of $CH_3NH_3PbI_{3-x}Cl_x$ PVs have already exceeded 15%[14,24,25] thanks to the evolution of material and device engineering, however, the underlying mechanism that leads to the conversion of the precursors to the perovskite is not clear. In particular, it is widely reported that the $CH_3NH_3PbI_{3-x}Cl_x$ films show the same characteristic X-ray diffraction (XRD) peaks as the $CH_3NH_3PbI_3$ films, suggesting that the two compounds possess identical crystal lattices. Accordingly, only very low chlorine (Cl) content should be present in $CH_3NH_3PbI_{3-x}Cl_x$, because otherwise the lattice distortion induced by Cl atoms will cause shift and broadening of the XRD peaks. Therefore a fundamental question remains regarding the function of Cl atoms during the formation process of the perovskite.

Here we investigated this question through a combination of chemical, morphological, structural and thermal analyses. The energy dispersive X-ray spectrometry (EDX) and surface-sensitive X-ray photoelectron spectroscopy (XPS) depth profile reveal unambiguously the negligible amount of Cl atoms in the $CH_3NH_3PbI_{3-x}Cl_x$ compound. A polymer/perovskite/FTO glass

H. Yu, Dr. F. Wang, W. Li, Prof. N. Zhao
Department of Electronic Engineering
The Chinese University of Hong Kong
New Territories, Hong Kong
E-mail: nzhao@ee.cuhk.edu.hk
Prof. F. Xie, Prof. J. Chen
Instrumental Analysis and Research Center
Sun Yat-sen University
Guangzhou 510275, P. R. China

DOI: 10.1002/adfm.201401872

testing structure is applied to study the thermal annealing process, and the results show that the formation of the perovskite is likely accompanied by release of gaseous CH_3NH_3Cl (or other organic chlorides in a similar form) through an intermediate organometal mixed halide phase. Based on the observation we further compared the $MAPbX_3$ films produced from $CH_3NH_3I/PbCl_2$ and CH_3NH_3I/PbI_2 precursor combinations with different molar ratios. The results demonstrate that the initial introduction of a $CH_3NH_3^+$ rich environment is critical to slow down the perovskite formation process and thus improve the growth of the crystal domains during annealing and that the function of Cl is to facilitate the release of excess $CH_3NH_3^+$ at a relatively low annealing temperature.

2. Results and Discussion

2.1. Elemental Analysis of Mixed Halide Perovskite

The mixed halide perovskite ($CH_3NH_3PbI_{3-x}Cl_x$) films were prepared in a nitrogen filled glove box by spin-coating a precursor solution of CH_3NH_3I and $PbCl_2$ in DMF at a 3:1 molar ratio, followed by thermal annealing at 100 °C for 50 min.

The scanning electron microscope (SEM) image in **Figure 1**a demonstrates a full coverage of the annealed perovskite film on an FTO substrate. The elemental composition of the annealed film was analyzed by X-ray photoelectron spectroscopy (XPS). A full spectrum scan from the top surface of the film shows no trace of Cl in the perovskite (Figure 1b). Since the detection depth of XPS is limited to a few tens of nm, we further performed XPS depth profile measurement by sputtering the perovskite films with Ar ion gun (EX05 Ion Gun). As shown in Figure 1c, no signal related to the Cl 2p electrons is found in the bulk perovskite film (around 310 nm thick); very weak Cl signal, which corresponds to 1% Cl, can be detected for the top 20 nm of the film.

The XPS analysis clearly suggests that there is negligible amount of Cl atoms in the fully annealed perovskite film. Therefore, one can speculate that Cl atoms escape from the film during the annealing process, most likely in the form of gaseous Cl-containing compounds. Although Cl does not exist in the final product of the perovskite film, the use of the Cl-containing precursor seems to play an important role in determining the electronic properties of the perovskite thin films. The time-resolved photoluminescence study by Snaith et al.[26] shows that the $MAPbX_3$ perovskite films prepared from the $CH_3NH_3I/PbCl_2$ precursors exhibit longer charge carrier diffusion lengths as compared to those prepared from the CH_3NH_3I/PbI_2. In order to understand how the Cl involved reaction affects the properties (e.g., crystallinity and preferred

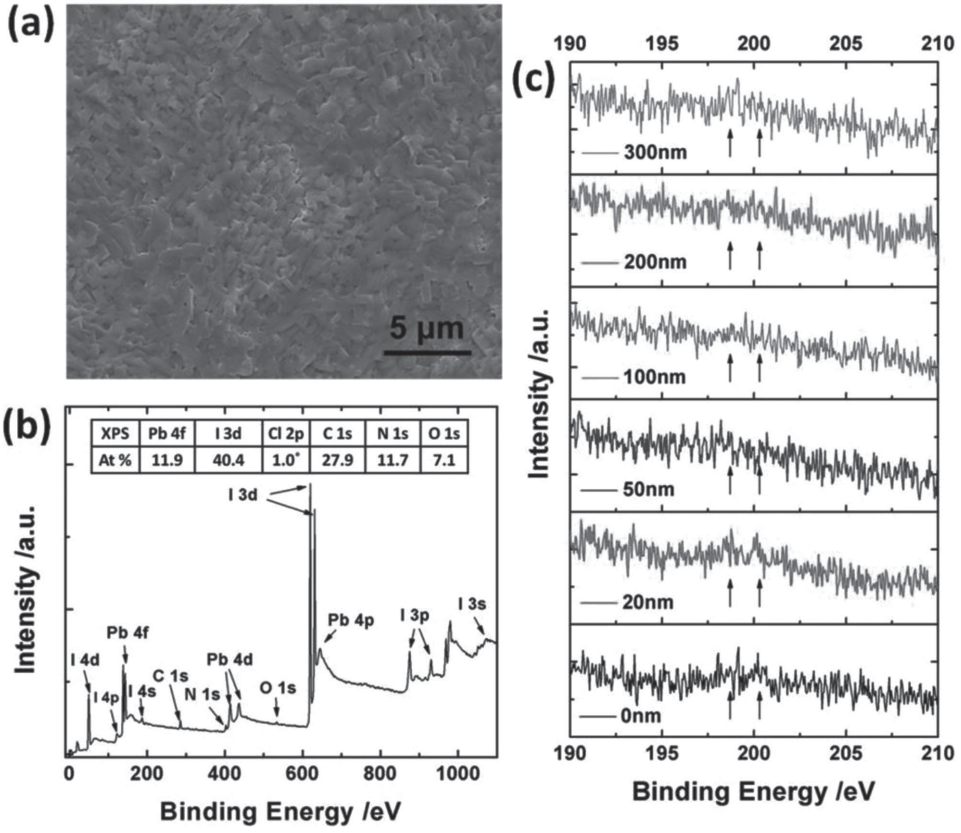

Figure 1. a) Morphology of the mixed halide perovskite ($CH_3NH_3PbCl_xI_{3-x}$) films on FTO substrates by SEM; b) XPS survey spectrum of the top surface of the mixed halide perovskite ($CH_3NH_3PbCl_xI_{3-x}$) film; *Atomic percentage was calculated from the high resolution XPS spectra; c) Cl2p core level XPS spectra under Ar ion gun sputtering on the perovskite film, characteristic peak binding energy of $Cl2p_{3/2}$ and $Cl2p_{1/2}$ (198.9 eV and 200.5 eV) highlighted by the arrows. "0 nm" means the top surface of the perovskite film before Ar ion gun sputtering, and other values (e.g., 20 nm, 50 nm, 100 nm, etc.) refer to the gradually increased thickness of the removed perovskite during sputtering.

Adv. Funct. Mater. **2014**,
DOI: 10.1002/adfm.201401872

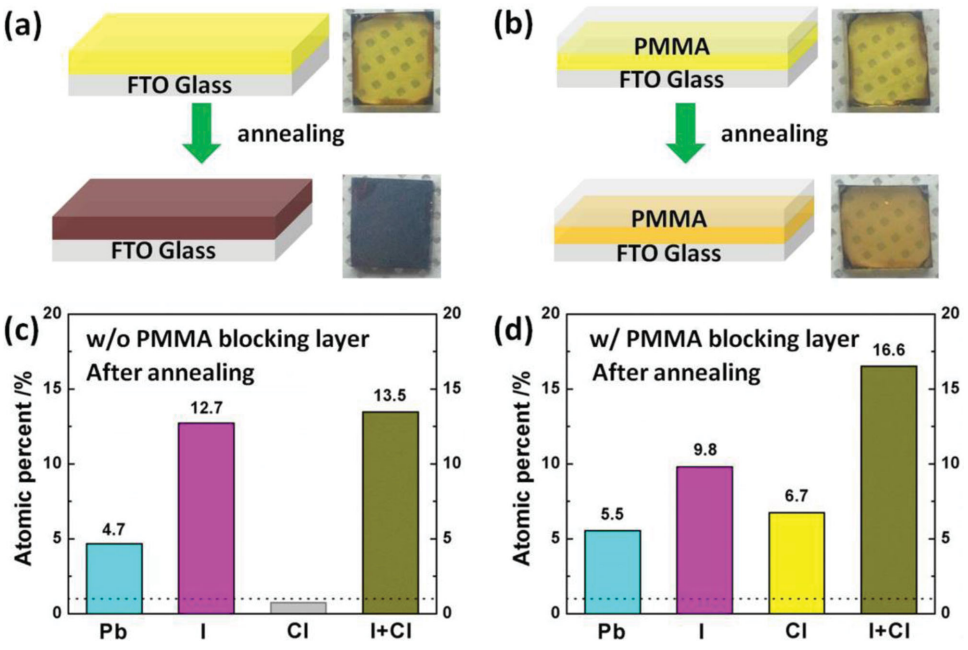

Figure 2. Schematics and photos of a) perovskite/FTO and b) PMMA/perovskite/FTO structures before (top) and after (bottom) annealing. EDX measured atomic percentages of the main elements (Pb, I and Cl) in the annealed perovskite films c) without and d) with the PMMA blocking layer.

orientation) of the $MAPbX_3$ perovskite films, we further examined the formation process of the so-called mixed halide perovskite through thermal and elemental analysis.

2.2. Formation Process of Mixed Halide Perovskite

Figure 2 illustrates a comparative study on the annealing process of two $MAPbX_3$ perovskite films, where one precursor film was spun on an FTO substrate (Figure 2a) and the other was sandwiched between FTO and a 200 nm thick polymethyl methacrylate (PMMA) layer (Figure 2b). Color variation is a straightforward indicator for the progress of the chemical reaction occurring during the annealing process. For the perovskite/FTO structure, a color change from yellow to dark brown was observed after annealing at 100 °C for 50 min, and the full formation of the perovskite phase was also confirmed by the X-ray diffraction (XRD) measurement. In contrast, the PMMA/perovskite/FTO structure exhibits only a slight color change, indicating that the reaction to form perovskite was suppressed. The elemental composition of both structures was analyzed using energy dispersive X-ray (EDX) spectroscopy. For the perovskite film without the PMMA blocking layer, there is a negligible trace of Cl in the film, as shown in Figure 2c. (Note that the measured atomic percentage of 0.7% for Cl is lower than the detection limit of ≈1% for the EDX setup.) For the FTO/perovskite/PMMA structure, however, the atomic percentage for Cl is 6.7%, and the atomic ratio of Cl to (Cl +I) is around 0.4 (Figure 2d), which is the same as the ratio in the precursor solution. Therefore it is likely that the reaction from the precursor phase to perovskite phase requires release of gaseous Cl-containing compound(s), a process that is largely suppressed by the PMMA blocking layer. (We note that PMMA is not a perfect gas barrier. However, the color of the FTO/perovskite/PMMA structure changes little even after 6 hours' annealing, suggesting that the release of the gas molecules is a very slow process.)

The above experiment clearly suggests that the release of the Cl-containing compound(s) is closely linked to the formation of crystalline $MAPbX_3$ perovskite films. It is therefore important to understand the possible chemical reactions involved in the perovskite formation process. Dualeh et al. proposed that Reaction (1) in **Scheme 1** dominates the annealing process.[22] However, we note that the initial CH_3NH_3I and $PbCl_2$ compounds appear to be white, while their DMF solution mixture produces a precursor film with light yellow color (Figure 2a), indicating that a chemical reaction must occur to form a new precursor phase. Hence, Reaction (1) may involve several intermediate steps. Firstly, since the amount of CH_3NH_3I in molar is 3 times that

Reaction (1):

$$PbCl_2 + 3CH_3NH_3I \rightarrow CH_3NH_3PbI_3 + 2CH_3NH_3Cl(g)\uparrow$$

Reaction (2):

(2-1) $$PbCl_2 + 3CH_3NH_3I \rightarrow PbI_2 + CH_3NH_3I + 2CH_3NH_3Cl$$

(2-2) $$PbI_2 + CH_3NH_3I + 2CH_3NH_3Cl \rightarrow CH_3NH_3PbI_3 + 2CH_3NH_3Cl(g)\uparrow$$

(2-3) $$PbI_2 + xCH_3NH_3I + yCH_3NH_3Cl \rightarrow (CH_3NH_3)_{x+y}PbI_{2+x}Cl_y \text{ (Intermediate phase)}$$
$$\rightarrow CH_3NH_3PbI_3 + CH_3NH_3Cl(g)\uparrow$$

Scheme 1. Possible chemical reactions involved in the perovskite formation process.

of $PbCl_2$, Reaction (2–1) is proposed, where part of CH_3NH_3I reacts with $PbCl_2$ to form PbI_2. As a result of Reaction (2–1), the as-spun film contains a mixture phase of PbI_2 (appears in light yellow), CH_3NH_3I, CH_3NH_3Cl, and possibly some unreacted $PbCl_2$. During annealing two reaction processes may occur: For Reaction (2–2), CH_3NH_3I reacts with PbI_2 to form the dark brown $CH_3NH_3PbI_3$ perovskite; meanwhile, the excess CH_3NH_3Cl escapes from the film through either sublimation or decomposition into other gaseous Cl-containing mixtures. For Reacton (2–3), an intermediate phase forms during spin-coating or the early stage of the annealing process. In this case, the $CH_3NH_3PbI_3$ perovskite crystal domains grow during the decomposition of the intermediate phase, which is driven by the release of gaseous CH_3NH_3Cl (or other organic chlorides).

In order to find out whether Reaction (2–2) or Reaction (2–3) dominates the formation of $CH_3NH_3PbI_3$ perovskite, we performed XRD measurement on 5- and 15-min annealed precursor films to observe the intermediate products of the reaction. The XRD measurement was performed in ambient conditions (60% humidity level), and a 300 nm CYTOP (a fluorinated polyether) layer was covered on the samples to slow down the penetration of water molecules in air. As shown in the XRD spectra in **Figure 3**, two perovskite peaks at 14.2° and 28.5° can be readily observed in the freshly made 5- and 15-minutes annealed films, although the peak intensity is relatively small.

The peaks at 12.7° and 17.5° correspond to PbI_2 and CH_3NH_3Cl, respectively. Two strong peaks at 15.7° and 31.5° can be seen initially but drops quickly after exposure of the films in air for a few minutes, accompanied by the growth of the perovskite peaks. In previous studies, the 15.7° and 31.5° peaks are correlated to the (100) and (200) diffractions of a $CH_3NH_3PbCl_3$ single crystal phase grown in an aqueous solution.[27,28] However, such assignment could not explain the disappearance of the "$CH_3NH_3PbCl_3$" phase after air exposure.

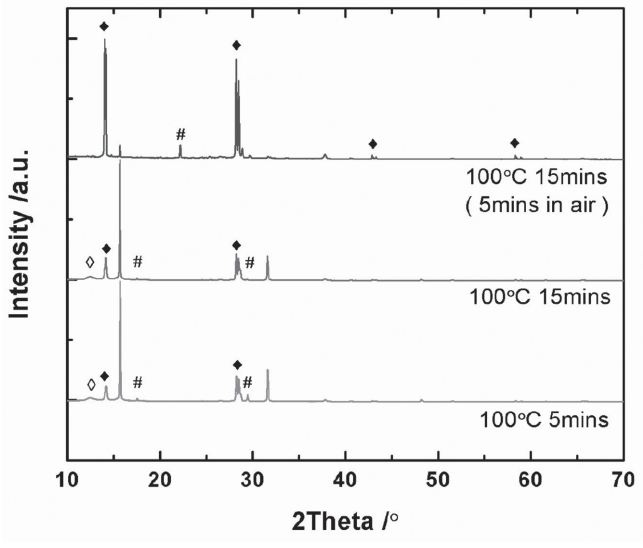

Figure 3. XRD patterns for the precursor films annealed for 5 mins and 15 mins. ♦, ◊ and # denote the peaks of $CH_3NH_3PbI_3$ perovskite, PbI_2, and CH_3NH_3Cl, respectively; the unlabelled peaks are attributed to the intermediate phase.

We therefore suspect that the 15.7° and 31.5° peaks may originate from another $(CH_3NH_3)_{x+y}PbI_{2+x}Cl_y$ phase or a mixture of several phases. To unambiguously identify the intermediate reaction products, a combination of in situ XRD and XPS measurements in vacuum would be critical. Such study is currently undergoing. It's worth mentioning that there have been several reports recently to study the intermediate phase structures.[29,30]

2.3. Comparison Between $CH_3NH_3PbI_3$ Perovskites Formed from $CH_3NH_3I/PbCl_2$ and CH_3NH_3I/PbI_2 Precursor Mixtures

Since the amount of Cl in $CH_3NH_3PbI_{3-x}Cl_x$ is negligible, it is more precise to write the formula of the perovskite as $CH_3NH_3PbI_3$. Although at present the exact formation reaction of $CH_3NH_3PbI_3$ cannot be identified, one can still explore the role of Cl by comparing the formation processes of the perovskites from the $CH_3NH_3I/PbCl_2$ and CH_3NH_3I/PbI_2 precursor combinations. Firstly, we note that due to the better solubility of PbI_2, the CH_3NH_3I/PbI_2 precursor solution can be made at a 1:1 molar ratio. (In contrast, a 3:1 molar ratio is required for $CH_3NH_3I/PbCl_2$). A $CH_3NH_3PbI_3$ perovskite film is obtained by spin coating the precursor solution on an FTO substrate, followed by only 10 minutes' annealing at 100 °C. In this case, however, there are large voids formed in the perovskite film (Figure S1, Supporting Information), and changing the annealing time and temperature cannot improve the film quality. We note that previous studies have demonstrated high performance planar PVs with closely packed crystalline $CH_3NH_3PbI_3$ films fabricated from the CH_3NH_3I/PbI_2 precursor combination. For instance, PCEs of over 15% and 12% are achieved through a sequential deposition method[18] and vapor-assisted solution process,[19] respectively. In both cases, a CH_3NH_3I-rich environment was provided, suggesting that excess CH_3NH_3I could be beneficial to the formation of high quality $CH_3NH_3PbI_3$ films.

We therefore monitored the film morphology as a function of the CH_3NH_3I:PbI_2 molar ratio. Notably, as the molar ratio increases to 2:1 or above, the annealing condition has to be adjusted to 150 °C for 20 minutes to ensure full conversion of the precursors to the perovskite phase (Analysis of the incompletely converted precursor films annealed at lower temperatures is provided in Figure S2,S3 in Supporting Information). Only by reducing the film thickness to < 200 nm, the annealing temperature can be lowered to 130 °C. (Note that the thickness of the CH_3NH_3I:$PbCl_2$ produced films is around 310 nm). **Figure 4** shows the SEM images of the annealed perovskite films obtained from the CH_3NH_3I:PbI_2 precursor mixtures with different molar ratios.

It can be seen that uniform and compact perovskite films are obtained when the molar ratio exceeds 2:1. Furthermore, the 2:1 and 3:1 films also exhibit stronger preferred orientation along (110), as revealed by the XRD measurement (**Figure 5**). Interestingly, these structural characteristics are very similar to those of the perovskite phase prepared from the Cl-containing precursors (CH_3NH_3I:$PbCl_2$) with 3:1 molar ratio. Nevertheless, the PV performances of the two perovskite phases are very different in a planar device structure (FTO/compact TiO_2/ Perovskite/P3HT/Ag) (Figure S4, Supporting Information): the 100 °C annealed

DOI: 10.1002/adfm.201401872

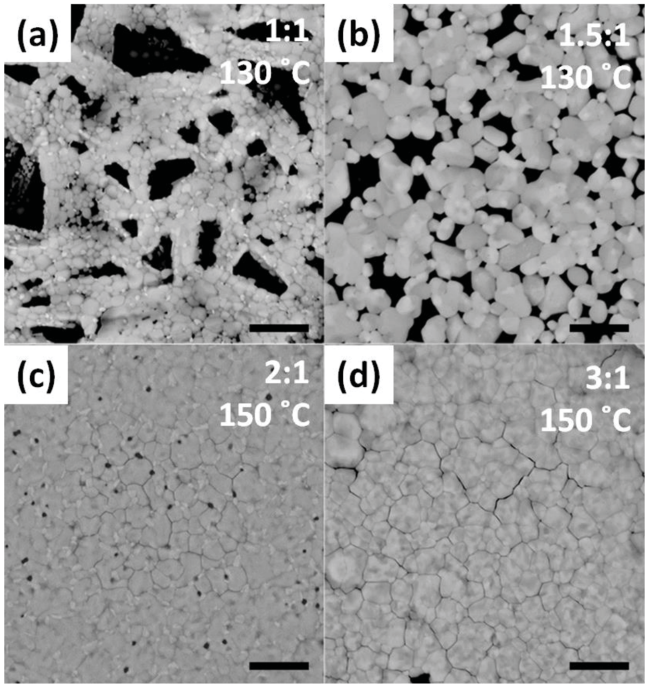

Figure 4. SEM images of annealed perovksite films obtained from CH_3NH_3I:PbI_2 precursor mixtures with a) 1:1, b) 1.5:1, c) 2:1, d) 3:1 molar ratios. Scar bar: 3 μm.

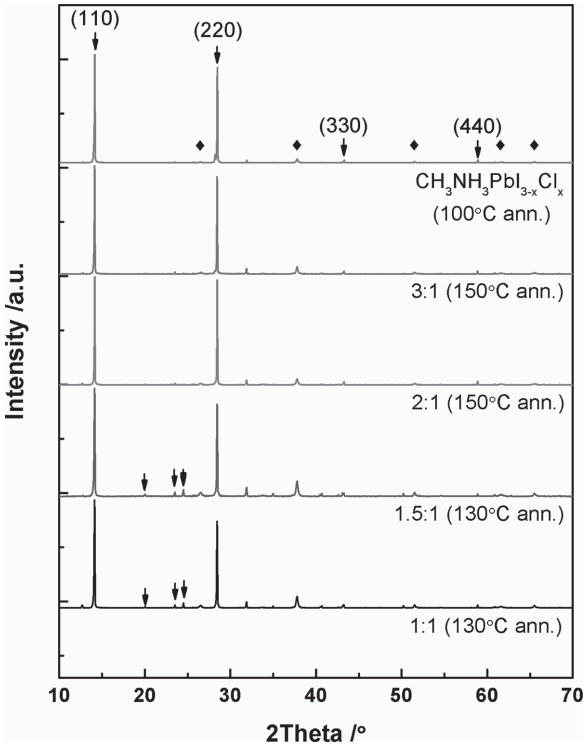

Figure 5. XRD patterns for the fully annealed perovksite films obtained from the CH_3NH_3I:PbI_2 precursor mixtures with different molar ratios. Small peaks at 20–30° (highlighted by arrows) correspond to (200), (211), and (202) diffractions in the films with CH_3NH_3I:PbI_2 ratios of 1:1 and 1.5:1, indicating more randomly oriented crystal domains.

perovskite formed from CH_3NH_3I:$PbCl_2$ exhibits a PCE of ≈12%, whereas the 150 °C annealed perovskite formed from 2:1 and 3:1 CH_3NH_3I:PbI_2 with a comparable thickness yields <2% PCE in the same device configuration. The 130 °C annealed thin perovskite formed from 2:1 CH_3NH_3I:PbI_2 (optimized for PV performance) yields ≈8% PCE. In this case, although the reduction in the annealing temperature leads to a better PV performance, the thin film thickness limits the light absorption and thus the generation of photocurrent in the perovskite.

The above morphological and structural studies of the perovskite formation process suggest that the use of excess CH_3NH_3X (X: Cl or I) can slow down the formation and crystallization of the perovskite, possibly through the introduction of certain intermediate phases. This principle works for both pure iodine precursors (CH_3NH_3I/PbI_2) as well as mixed halide precursors (CH_3NH_3I/$PbCl_2$), and can be used to obtain dense, uniform and highly crystalline perovskite films. On the other hand, the species of the precursors could largely affect the annealing temperature. The CH_3NH_3I/$PbCl_2$ (3:1 molar ratio) combination only requires 100 °C annealing to achieve full conversion to perovskite; while in the case of CH_3NH_3I/PbI_2 (3:1 molar ratio), the annealing temperature can be as high as 150 °C, due possibly to a higher energy required for the formation (or decomposition) of the intermediate phase or release of the gaseous I-containing compounds (e.g., CH_3NH_3I).

2.4. Thermal Behavior of CH_3NH_3I and CH_3NH_3Cl

Since the formation of the $CH_3NH_3PbI_3$ perovskites is significantly influenced by the release of methylammonium halides, we further characterized the thermal property of CH_3NH_3I and CH_3NH_3Cl via thermal gravimetric analysis (TGA) and differential scanning calorimetry (DSC) measurements. The reactions related to a weight loss of CH_3NH_3I and CH_3NH_3Cl could be monitored by the TGA measurement.

As shown in **Figure 6**a, the TGA curves show nearly 100% weight loss between 250 °C and 360 °C for CH_3NH_3Cl and between 290 °C and 370 °C for CH_3NH_3I, respectively. The lower onset of the weight loss temperature of CH_3NH_3Cl suggests that it is easier to turn into gaseous phase as compared to CH_3NH_3I. Note that the TGA measurement was performed on CH_3NH_3I and CH_3NH_3Cl powders. In the case of around 300 nm thick perovskite precursor films, a much larger surface-to-volume ratio is provided; therefore the sublimation temperature could be considerably lower than 250–300 °C. (Directly performing the TGA measurement on thin film perovskite samples cannot yield reliable results due to the extremely low mass loss of the material as compared to the substrate.)

We further performed DSC measurement to understand in what manner CH_3NH_3Cl and CH_3NH_3I could possibly escape from the precursor films during the annealing process. In general, a sublimation process is endothermic, while a decomposition process is exothermic. As shown in Figure 6b, the endothermic peaks in the DSC curves suggest that the release of CH_3NH_3Cl and CH_3NH_3I is related to a sublimation process. Due to the uncertainty of the intermediate product in Reaction (2–3), we can only speculate that the release of the Cl atoms is in the form of gaseous CH_3NH_3Cl. Both the TGA and DSC

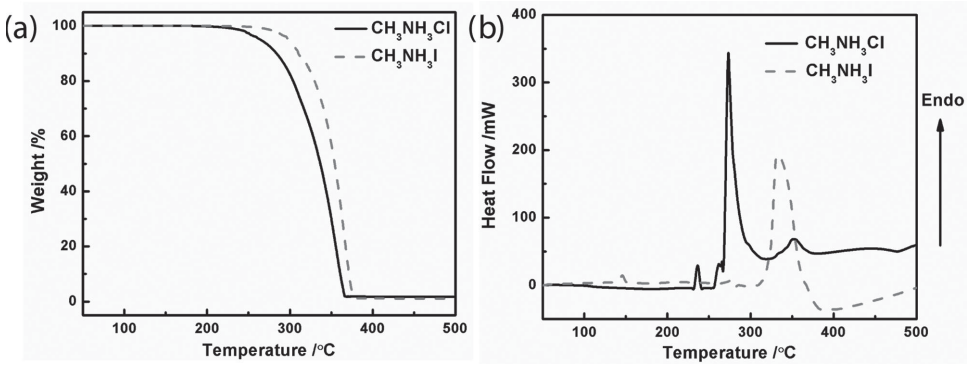

Figure 6. a) TGA and b) DSC curves for CH_3NH_3I and CH_3NH_3Cl powders.

results confirm that the release of CH_3NH_3I occurs at higher temperature as compared to CH_3NH_3Cl, which may explain the higher annealing temperature required for the CH_3NH_3I/PbI_2 precursor mixtures. Therefore we propose that the function of Cl (or more precisely, Cl^-) is to facilitate the release of excess $CH_3NH_3^+$ at a relatively low annealing temperature.

3. Conclusion

In summary, we have shown by EDX and XPS depth-profile that only negligible amount of Cl atoms exist in the fully annealed, so-called "mixed halide" perovskite ($CH_3NH_3PbI_{3-x}Cl_x$) films. By monitoring the annealing products in the perovskite/FTO and PMMA/perovskite/FTO testing structures we found that the slow formation of the $CH_3NH_3PbI_{3-x}Cl_x$ perovskite is likely driven by release of gaseous CH_3NH_3Cl (or other organic chlorides in a similar form) through an intermediate organolead mixed halide phase. Furthermore, by comparing the perovskite films produced from $CH_3NH_3I/PbCl_2$ and CH_3NH_3I/PbI_2 precursor combinations with different molar ratios, we demonstrated that the initial introduction of a $CH_3NH_3^+$ rich environment is critical to slow down the perovskite formation process and thus improve the growth of the crystal domains during annealing; accordingly, the function of Cl is to allow the removal of excess $CH_3NH_3^+$ at a relatively low annealing temperature. Our study reveals the importance of controlling the formation reaction of perovskites. The method of using mixed halide precursors to tune the annealing process can be extended to other organometal perovskite material systems.

4. Experimental Section

Preparation of Perovskite Precursor: CH_3NH_3I was synthesized in an ice bath for 2 hrs by reacting methylamine (CH_3NH_2, 33 wt% in ethanol from Sigma-Aldrich) with hydroiodic acid (HI, 57 wt% in water from Sigma-Aldrich). The white powders were precipitated by drying at 60 °C and washed for 3 times with diethyl ether (Sigma-Aldrich) before further dried out to be stored in nitrogen-filled glove-box. CH_3NH_3Cl was synthesized in the same way as CH_3NH_3I by reacting methylamine with hydrochloric acid (HCl, 36.5–38 wt% in water from Sigma-Aldrich). $CH_3NH_3PbI_{3-x}Cl_x$ precursor solution was prepared by dissolving 0.88M lead chloride (99.999%, Sigma-Aldrich) and 2.64 M CH_3NH_3I in anhydrous *N,N*-Dimethylformamide (DMF, 99.8%, Sigma-Aldrich). Similarly, $CH_3NH_3PbI_3$ precursor solutions were prepared by dissolving 0.9 M lead iodide (99.999%, Sigma-Aldrich) and 0.9 M for 1:1, 1.35M for 1.5:1, 1.8 M for 2:1, 2.7 M CH_3NH_3I for 3:1 in anhydrous DMF. The precursor solutions were filtered though a 0.2 μm PTFE filter before spin-coating.

Fabrication of Polymer/Perovskite/FTO Glass Sandwiched Structure Test Samples: The whole process was carried out in a nitrogen filled glovebox. $CH_3NH_3PbI_{3-x}Cl_x$ precursor solution was first spin-coated on a FTO glass. After drying over-night, a 40 mg/mL poly(methyl methacrylate) (PMMA, Mw of 120000, purchased from Sigma-Aldrich) solution in butyl acetate (anhydrous, 99%, Sigma-Aldrich) was then spin-coated on the perovskite film either before or after annealing.

Fabrication of Planar Solar Cell Devices: Solar cells were fabricated as follows: FTO (DHS-FTO22–15N, HeptaChroma) substrates were sequentially cleaned with deionized water, acetone, 2-propanol for 30 mins each, followed with oxygen plasma treatment for 1.5 mins. A compact TiO_2 hole-block layer was deposited on cleaned FTO by spin-coating a mildly acidic solution of titanium butoxide (97%, Sigma-Aldrich) in ethanol (consisting of 0.5 mL titanium butoxide and 50 μL 37% HCl solution in 6 ml ethanol) at 5000 rpm for 25s, and annealed at 500 °C for 45 min in an oven. Then TiO_2 coated FTO substrates were transferred into a nitrogen-filled glovebox and pre-heated at 100 °C for 10 min. After the substrates were cooled to room temperature, the perovskite precursor solution was spin-coated at 3000 r.p.m. for 60 s. After drying for more than 10 mins, the as spun films were annealed for 50 mins at 100 °C in the case of $CH_3NH_3PbI_{3-x}Cl_x$ and at 130 °C for 20 min (or 150 °C for 20 min) in the cases of CH_3NH_3I/PbI_2 at molar ratios of 2:1 and 3:1. 30nm P3HT (Poly(3-hexylthiophene-2,5-diyl), LT-S909 from Lumtec.) hole transport layer was deposited on the annealed perovskite film by spin-coating 15 mg/ml P3HT solution in chlorobenzene at 3000 r.p.m. for 60 s. Finally, 100 nm Ag electrodes were thermally evaporated through a shadow mask under a vacuum of 1×10^{-6} Torr to complete the device fabrication.

Characterizations: Morphology of the perovskite films were observed by HR-FESEM (FEI, Quanta 400). The elemental composition in the films was measured by EDX with Standardless Quantification Model and by XPS (Thermo Fisher Scientific, ESCALAB 250). The crystalline structure for the perovskite films were identified by XRD (Rigaku, SmartLab). Thermal analyses for CH_3NH_3I and CH_3NH_3Cl powders were carried out by Thermogravimetric Analyzer (PerkinElmer, TGA 6) and DSC (PerkinElmer, TGA 6). Sample thicknesses were measured using an Alpha step 500 Surface profiler. The current density–voltage (*J–V*) curves were measured (Keithley Instruments, 2612 Series SourceMeter) under simulated AM 1.5 sunlight at 100 mW cm^{-2} irradiance generated by an 94011A-ES Sol series Solar Simulator.

Supporting Information

Supporting Information is available from the Wiley Online Library or from the author.

DOI: 10.1002/adfm.201401872

Acknowledgements

The authors gratefully acknowledge the fundings from Research Grants Council of Hong Kong (Grants No. CUHK419311 and T23–407/13-N), National Natural Science Foundation of China (Grants No. 61205036 and 51303217) and Shun Hing Institute of Advanced Engineering (Grant no. 8115041).

Received: June 8, 2014
Revised: August 7, 2014
Published online:

[1] N. G. Park, *J. Phys. Chem. Lett.* **2013**, *4*, 2423.
[2] H. J. Snaith, *J. Phys. Chem. Lett.* **2013**, *4*, 3623.
[3] R. F. Service, *Science* **2014**, *344*, 458.
[4] S. Kazim, M. K. Nazeeruddin, M. Grätzel, S. Ahmad, *Angew. Chem. Int. Ed.* **2014**, *53*, 2812.
[5] L. Etgar, P. Gao, Z. Xue, Q. Peng, A. K. Chandiran, B. Liu, M. K. Nazeeruddin, M. Grätzel, *J. Am. Chem. Soc.* **2012**, *134*, 17396.
[6] O. Malinkiewicz, A. Yella, Y. H. Lee, G. M. Espallargas, M. Graetzel, M. K. Nazeeruddin, H. J. Bolink, *Nat. Photonics* **2014**, *8*, 128.
[7] M. M. Lee, J. Teuscher, T. Miyasaka, T. N. Murakami, H. J. Snaith, *Science* **2012**, *338*, 643.
[8] J. M. Ball, M. M. Lee, A. Hey, H. J. Snaith, *Energy Environ. Sci.* **2013**, *6*, 1739.
[9] J. H. Noh, S. H. Im, J. H. Heo, T. N. Mandal, S. I. Seok, *Nano Lett.* **2013**, *13*, 1764.
[10] E. Edri, S. Kirmayer, M. Kulbak, G. Hodes, D. Cahen, *J. Phys. Chem. Lett.* **2014**, *5*, 429.
[11] E. Edri, S. Kirmayer, A. Henning, S. Mukhopadhyay, K. Gartsman, Y. Rosenwaks, G. Hodes, D. Cahen, *Nano Lett.* **2014**, *14*, 1000.
[12] E. Edri, S. Kirmayer, S. Mukhopadhyay, K. Gartsman, G. Hodes, D. Cahen, *Nat. Commun.* **2014**, *5*.
[13] V. Gonzalez-Pedro, E. J. Juarez-Perez, W.-S. Arsyad, E. M. Barea, F. Fabregat-Santiago, I. Mora-Sero, J. Bisquert, *Nano Lett.* **2014**, *14*, 888.
[14] M. Liu, M. B. Johnston, H. J. Snaith, *Nature* **2013**, *501*, 395.
[15] J. B. You, Z. R. Hong, Y. Yang, Q. Chen, M. Cai, T. B. Song, C. C. Chen, S. R. Lu, Y. S. Liu, H. P. Zhou, Y. Yang, *ACS Nano* **2014**, *8*, 1674.
[16] B. Conings, L. Baeten, C. De Dobbelaere, J. D'Haen, J. Manca, H.-G. Boyen, *Adv. Mater.* **2014**, *26*, 2041.
[17] P.-W. Liang, C.-Y. Liao, C.-C. Chueh, F. Zuo, S. T. Williams, X.-K. Xin, J. Lin, A. K. Y. Jen, *Adv. Mater.* **2014**, *26*, 3748.
[18] D. Y. Liu, T. L. Kelly, *Nat. Photonics* **2014**, *8*, 133.
[19] Q. Chen, H. Zhou, Z. Hong, S. Luo, H.-S. Duan, H.-H. Wang, Y. Liu, G. Li, Y. Yang, *J. Am. Chem. Soc.* **2014**, *136*, 622.
[20] G. E. Eperon, V. M. Burlakov, P. Docampo, A. Goriely, H. J. Snaith, *Adv. Funct. Mater.* **2014**, *24*, 151.
[21] J. J. Choi, X. Yang, Z. M. Norman, S. J. L. Billinge, J. S. Owen, *Nano Lett.* **2014**, *14*, 127.
[22] A. Dualeh, N. Tétreault, T. Moehl, P. Gao, M. K. Nazeeruddin, M. Grätzel, *Adv. Funct. Mater.* **2014**, *24*, 3250.
[23] M. Saliba, K. W. Tan, H. Sai, D. T. Moore, T. Scott, W. Zhang, L. A. Estroff, U. Wiesner, H. J. Snaith, *J. Phys. Chem. C* **2014**, *118*, 17171.
[24] J. T.-W. Wang, J. M. Ball, E. M. Barea, A. Abate, J. A. Alexander-Webber, J. Huang, M. Saliba, I. Mora-Sero, J. Bisquert, H. J. Snaith, R. J. Nicholas, *Nano Lett.* **2014**, *14*, 724.
[25] J. Burschka, N. Pellet, S.-J. Moon, R. Humphry-Baker, P. Gao, M. K. Nazeeruddin, M. Grätzel, *Nature* **2013**, *499*, 316.
[26] S. D. Stranks, G. E. Eperon, G. Grancini, C. Menelaou, M. J. P. Alcocer, T. Leijtens, L. M. Herz, A. Petrozza, H. J. Snaith, *Science* **2013**, *342*, 341.
[27] O.-Y. Noriko, T. Matsuo, H. Suga, *J. Phys. Chem. Solids* **1990**, *51*, 1383.
[28] O.-Y. Noriko, T. Matsuo, H. Suga, *J. Phys. Chem. Solids* **1992**, *53*, 935.
[29] K. W. Tan, D. T. Moore, M. Saliba, H. Sai, L. A. Estroff, T. Hanrath, H. J. Snaith, U. Wiesner, *ACS Nano* **2014**, *8*, 4730.
[30] Y. Zhao, K. Zhu, *J. Phys. Chem. C* **2014**, *118*, 9412.